Communications

Rigorous Analysis of Radiation Properties of Lossy Patch Resonators on Complex Anisotropic Media and Lossy Ground Metallization

Zhenglian Cai and Jens Bornemann

Abstract—**An extended spectral-domain immittance approach for the rigorous analysis of resonant frequencies and radiation characteristics of microstrip resonators is presented. The dyadic Green's function in the spectral domain is modified to include a complex anisotropic substrate with both permeability and permittivity tensors, lossy ground metallization, and a lossy conducting patch of conventional or superconducting material. Closed-form expressions for the transverse propagation constants and related immittances of TE and TM waves in the spectral domain lead to a CPU-time efficient algorithm that is operational on standard workstations. Numerical results show how the radiation characteristics are affected by losses as well as uniaxial and biaxial anisotropies.**

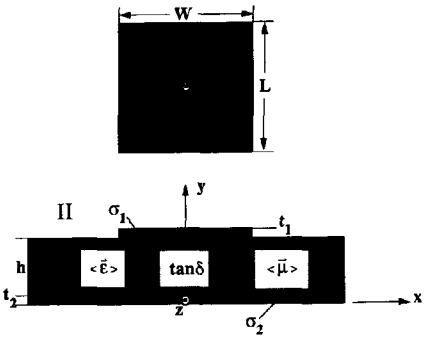

Fig. 1. Geometry of lossy patch radiator on anisotropic substrate and lossy ground metallization.

I. INTRODUCTION

With the evolution of material technology to a state that is currently found in modern MMIC's, the design of integrated radiating systems has become increasingly difficult. This is owing, first, to the anisotropic behavior of modern substrates, which affects the performance of circuits and printed antennas [1], and second, to the nonnegligible influences of conductor and ground metallizations on circuit characteristics. Therefore, theoretical models, which are able to rigorously include the related effects in the analysis, are—and will be—in heavy demand. Moreover, it is desirable that such models include possible applications of high-Tc superconductors, which have been shown to offer attractive solutions in microstrip antenna technology, e.g., [2].

Several numerical methods for the calculation of characteristics and applications of anisotropic substrates for microstrip antennas have been introduced. Among those are the full-wave techniques proposed in, e.g., [3]–[5]. In [3], only the resonant frequency of a patch on uniaxial substrate is investigated. Although the method proposed in [4] includes the radiation properties of the antenna, it is also restricted to uniaxial substrates. It appears that the technique presented in [5] is able to solve the problem including a general anisotropic form. However, the paper lacks detailed numerical results both for the resonant frequency and for the radiation characteristics of the antenna. Some results applicable to high-Tc superconductor patch antennas are given in [6]. The theory includes the effects of conductors and ground metallizations but excludes those due to the anisotropy of the substrate. Furthermore, none of the above methods addresses the influences of different conductor materials and anisotropic substrates with ε and μ tensors on the radiation properties of patch radiators.

Therefore, this paper focuses on a rigorous technique for the resonant frequency and radiation pattern analysis of rectangular patch resonators. Although the fundamental approach is similar to [7] and [8], this contribution presents extensive modifications: first, the incorporation of the conductivity and finite thickness of the ground metallization, the properties of conventional or high-Tc superconducting patches, and two complex five-element tensors for electrically and magnetically anisotropic substrates; and second, the calculation of the radiation pattern as such. Our motivation is to provide the design engineer with a model that allows the investigation of possible influences on radiation characteristics due to anisotropies and losses of new materials, and that at the same time requires only standard workstations support instead of mainframe and/or vector computers.

Manuscript received December 3, 1992; revised October 12, 1993.

The authors are with the Centre of Advanced Materials and Related Technology (CAMTEC), Laboratory for Lightwave Electronics, Microwaves and Communications (LLiMiC), Department of Electrical and Computer Engineering, University of Victoria, Victoria B.C., Canada V8W 3P6.

IEEE Log Number 9404960.

II. THEORY

The geometry of a patch resonator with an imperfect conducting patch on an electrically and magnetically anisotropic substrate and lossy ground metallization is shown in Fig. 1. We restrict the demonstration of the procedure to the following five-component tensor cases:

$$\langle\bar{\varepsilon}\rangle = \varepsilon_0 \begin{bmatrix} \varepsilon_x & 0 & j\varepsilon_z \\ 0 & \varepsilon_y & 0 \\ -j\varepsilon_z & 0 & \varepsilon_x \end{bmatrix} \tag{1}$$

$$\langle\bar{\mu}\rangle = \mu_0 \begin{bmatrix} \mu_x & 0 & j\mu_z \\ 0 & \mu_y & 0 \\ -j\mu_z & 0 & \mu_x \end{bmatrix} \tag{2}$$

where $\mu_x, \mu_y, \mu_z, \varepsilon_x, \varepsilon_y$, and ε_z are complex quantities to account for the losses in the materials. The incorporation of tensors more general than those of (1) and (2) seems possible but has not yet been investigated.

The basic concept of the spectral-domain immittance approach (SDIA) as applied to ideal, infinitely thin conductors on conventional isotropic substrates is outlined in [9] and [10]. Therefore, only the basic steps and expressions inherent to the structure under investigation are presented here.

In order to decouple the hybrid electromagnetic field into TM and TE wave components, a coordinate transformation from the physical to the spectral domain is performed [9]. The key problem in case of anisotropic substrates is to separate TE-to-y and TM-to-y waves under the consideration of given material tensors. By solving

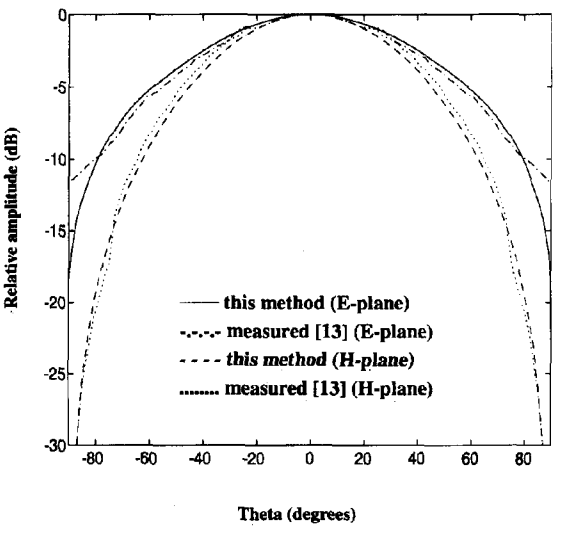

Fig. 2. Comparison of the results obtained by this method with measurements in [13]. Parameters: $W = 1.7$ cm, $L = 1.1$ cm, $h = 3.175$ mm, $t_1 = t_2 = 50$ μm, $\sigma = 56$ S/μm, $\varepsilon_x = 2.35$, $\varepsilon_y = 2.31$, $\varepsilon_z = 0$, $\tan\delta = 0.0012$, $\mu_x = \mu_y = 1$, $\mu_z = 0$.

Maxwell's equations in the spectral domain for the anisotropic region I (see Fig. 1), expressions for the complex propagation constants γ in y direction and respective wave admittances Y are readily obtained:

TM-to-y modes:

$$\gamma_m^2 = \frac{\varepsilon_x}{\varepsilon_y}(\alpha^2 + \beta^2 - k_0^2\varepsilon_y\mu_\perp) \tag{3}$$

$$Y_{\mathrm{TM}} = \frac{\varepsilon_x\varepsilon_\perp\omega(b\alpha - \beta)}{(j\varepsilon_x + \varepsilon_z b)\gamma_m(\beta + \alpha f)}. \tag{4}$$

TE-to-y modes:

$$\gamma_e^2 = \frac{\mu_x}{\mu_y}(\alpha^2 + \beta^2 - k_0^2\mu_y\varepsilon_\perp) \tag{5}$$

$$Y_{\mathrm{TE}} = -\frac{\gamma_e(\beta + d\alpha)(j\alpha\varepsilon_x + \beta\varepsilon_z)}{\varepsilon_x\omega\mu_0(j\mu_z + d\mu_x)(\alpha^2 + \beta^2)}. \tag{6}$$

In (3)–(6), α, β are the propagation constants in x, z directions, respectively. In fact, these quantities represent the variables in the spectral domain where, for each $\delta = \arccos\{\beta/\sqrt{\alpha^2 + \beta^2}\}$, waves may be decomposed into TM-to-y and TE-to-y [9]. k_0 is the free-space wave number, and the remaining abbreviations are given by

$$\mu_\perp = (\mu_x^2 - \mu_z^2)/\mu_x \quad \varepsilon_\perp = (\varepsilon_x^2 - \varepsilon_z^2)/\varepsilon_x \tag{7}$$

$$b = \frac{j\mu_x\alpha + \mu_z\beta}{\alpha\mu_z - j\beta\mu_x} \quad c = \frac{\varepsilon_z\alpha - j\beta\varepsilon_x}{j\alpha\varepsilon_x + \varepsilon_z\beta} \tag{8}$$

$$d = \frac{c\mu_z - j\mu_x}{\mu_z + jc\mu_x}$$

$$f = \frac{\varepsilon_y(j\beta\mu_x - \alpha\mu_z) + j\varepsilon_x(j\alpha\mu_x + \beta\mu_z)}{j\varepsilon_x(j\beta\mu_x - \alpha\mu_z) - \varepsilon_y(j\alpha\mu_x + \beta\mu_z)}. \tag{9}$$

Expressions for propagation constants and admittances of free-space region II (see Fig. 1) are well known.

By applying the spectral-domain immittance approach for imperfect conductors [5] and incorporating the surface impedances of conventional or superconductors [5], [7], [11] for the conducting patch as well as for the ground metallization, the spectral dyadic of the structure is obtained, e.g., [5]. After solving the system for the complex resonant frequency and the currents $\tilde{J}_x, \tilde{J}_z$, i.e., the Fourier transforms of current distributions J_x and J_z on the patch, the far-field pattern

$$E_\theta(\phi,\theta) \propto \sin\phi\tilde{E}_x(\alpha,\beta) + \cos\phi\tilde{E}_z(\alpha,\beta) \tag{10}$$

$$E_\theta(\phi,\theta) \propto \cos\phi\cos\theta\tilde{E}_x(\alpha,\beta) - \cos\theta\sin\phi\tilde{E}_z(\alpha,\beta) \tag{11}$$

with

$$\alpha = k_0\sin\phi\sin\theta \tag{12}$$

$$\beta = k_0\cos\phi\sin\theta \tag{13}$$

is obtained from $\tilde{E}_x$ and $\tilde{E}_z$,

$$\tilde{E}_x(\alpha,\beta,0) = [\tilde{Z}_{11}(\alpha,\beta) - Z_s]\tilde{J}_x(\alpha,\beta) + [\tilde{Z}_{12}(\alpha,\beta)]\tilde{J}_z(\alpha,\beta) \tag{14}$$

$$\tilde{E}_z(\alpha,\beta,0) = [\tilde{Z}_{21}(\alpha,\beta)\tilde{J}_x(\alpha,\beta) + [\tilde{Z}_{22}(\alpha,\beta) - Z_s]\tilde{J}_z(\alpha,\beta) \tag{15}$$

as they are the Fourier transforms of the electric fields. Such an approach avoids the evaluation of Sommerfeld-type integrals [10]. In (14) and (15), the quantites in brackets denote the spectral dyadic modified by the surface impedance Z_s of the patch. E-plane and H-plane patterns correspond to $\phi = 0$ (y–z plane), and $\phi = \pi/2$ (x–y plane), respectively (see Fig. 1).

For a given configuration, the computation time for both patterns is approximately 10 min on a IBM RS6000/530 workstation.

III. RESULTS

A comparison between the results obtained with this method and experimental data [13] is shown in Fig. 2. While only patch dimensions and substrate material are specified in [13], we have included conductor, ground plane, and substrate losses as well as some anisotropy typical for this kind of substrate. The plot is normalized to the maximum field strength. Close agreement between measurements and our computations is observed, particularly for the H plane. The agreement for the E-plane pattern is good up to angles of more than 80°, which is considered sufficient for the following investigations. The deviation at high angles is assumed to be attributed to the dispersion currents in the dielectric and the finite substrate size, which contribute to some radiation in z direction (Fig. 1) but are neglected in our model. In the H-plane pattern, this effects cannot be observed since currents at $x = \pm W/2$ are extremely small.

Fig. 3 shows the effect of different kind of losses on the radiation pattern. The normalization value in this plot (and all following ones) is the maximum calculated in the lossless case. In order to better distinguish between the two individual cases, the patterns are plotted on a linear amplitude scale. Case a shows the almost ideal case for a lossless substrate and a high-Tc superconducting patch. Resonance occurs at 8.15 GHz, and losses are negligible. Case b shows the combined effects of conventional patch, ground plane, and dielectric losses. The radiated field is below 90%, hence resulting in losses of almost 1 dB. The resonant frequency drops down to 8.12 GHz, due to effects of losses on the propagation constant, i.e., the wavelength. However, note that a fairly thick (3.15 mm) isotropic substrate with a loss tangent of 0.03 is considered here for demonstration purposes.

Fig. 4 demonstrates the effect of the electric anisotropic ratio on the radiation pattern. While different ratios $\varepsilon_x/\varepsilon_y$ have only little influence on the H-plane pattern (the results fall within the plotting accuracy of the solid curve), the E-plane beamwidth is significantly reduced with increasing electric anisotropic ratio. This is due to the electrically uniaxial substrate having identical dielectric constants in both planar directions (compare Fig. 1 and (1)). Consequently, the resonant frequency increases with anisotropic ratio (from 4.46 GHz to

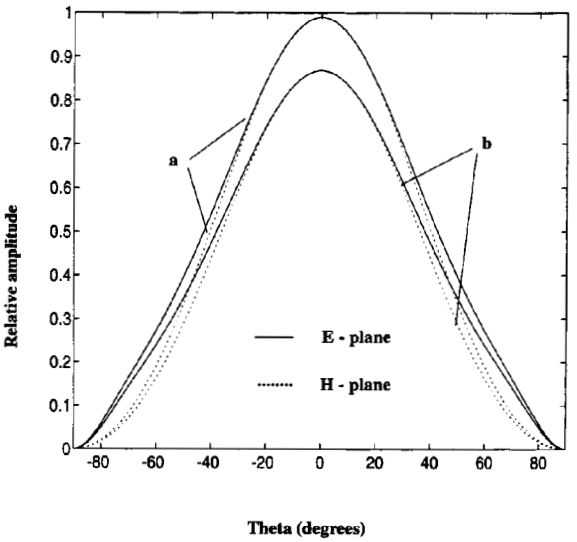

Fig. 3. The influence of different kinds of losses on the radiation pattern (amplitude normalized to maximum in lossless case). Parameters: $W = 1$ cm, $L = 1.2$ cm, $h = 3.15$ mm, $\varepsilon_x = \varepsilon_y = 2.3$, $\varepsilon_z = 0$, $\mu_x = \mu_y = 1$, $\mu_z = 0$. (a) Superconducting patch, ideal ground metallization; $t_1 = 0.3$ μm, $\sigma_n = 200$ S/mm, $T/T_c = 0.5$, $\lambda_{\text{eff}} = 1500$Å, $f_0 = 8.15$ GHz; (b) conventional conductor and ground plane, substrate losses included; $t_1 = t_2 = 35$ μm, $\sigma_1 = \sigma_2 = 40$ S/μm, $\tan\delta = 0.03$, $f_0 = 8.12$ GHz.

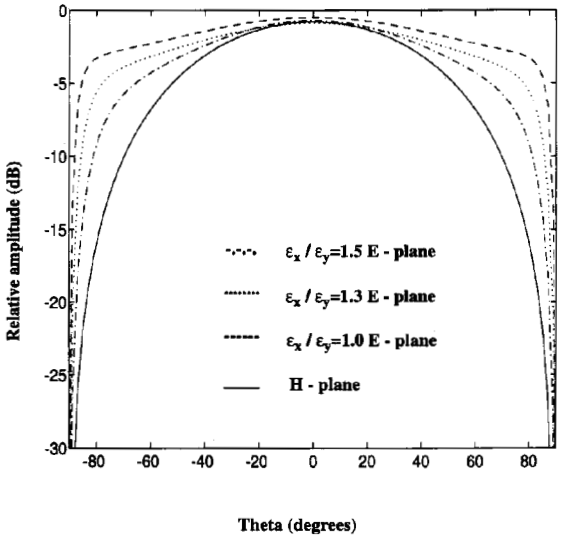

Fig. 4. Influence of electric anisotropic ratio on radiation pattern. Parameters: $W = 0.2$ cm, $L = 1.0$ cm, $h = 1.59$ mm, $\tan\delta = 0.002$,$t_1 = t_2 = 15$ μm, $\sigma_1 = \sigma_2 = 56$ S/μm, $\varepsilon_z = \mu_z = 0$, $\mu_x = \mu_y = 1$, $\varepsilon_x = 13.0$; dashed line: E plane $\varepsilon_x/\varepsilon_y = 1.0$, $f_0 = 4.46$ GHz; dotted line: E plane $\varepsilon_x/\varepsilon_y = 1.3$, $f_0 = 4.85$ GHz; dash-dotted line: E plane $\varepsilon_x/\varepsilon_y = 1.5$, $f_0 = 5.12$ GHz; solid line: H plane.

5.12 GHz). As the patterns are displayed at their respective resonant frequencies, the effective aperture increases with anisotropic ratio, thus reducing the beamwidth. Note that the isotropic case (dashed line) exhibits lowest losses.

As a practical example for purely magnetic biaxial anisotropy, Fig. 5 shows results of a patch antenna on ferrite substrate. The

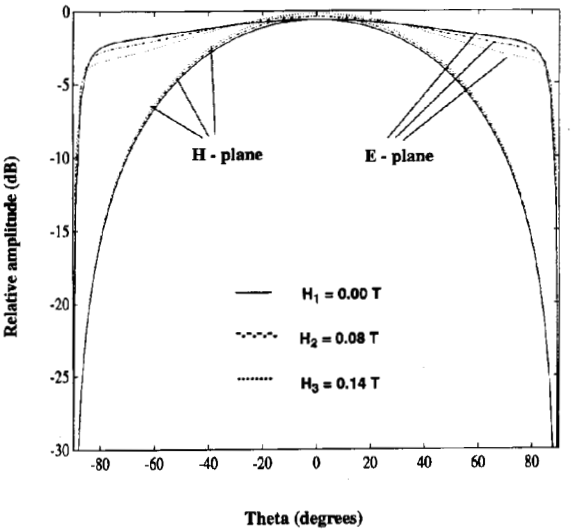

Fig. 5. Radiation pattern on patch radiator on ferrite substrate. Parameters: $W = 2.5$ mm, $L = 8$ mm, $h = 1$ mm, $\varepsilon_r = 16.6$, $\sigma_r = 0.0005$ S/m $H_s = 0.16$ T; superconducting patch: $t_1 = 0.5$ μm, $\sigma_n = 200$ S/mm, $T/T_c = 77/92.5$, $\lambda_{\text{eff}} = 1500$ Å; bottom metallization: $t_2 = 25$ μm, $\sigma_2 = 40$ S/μm; resonant frequencies for different dc magnetic bias: $f_1 = 6.48$ GHz, $f_2 = 7.81$ GHz, $f_3 = 9.08$ GHz.

variations of tensor parameters with externally applied dc magnetic field are incorporated according to well-known procedures [14]–[16]. Agreement with other methods in terms of propagation constants and loss factors has already been demonstrated in [7]. As expected for a magnetically tunable patch antenna, the radiation characteristics in both planes change only marginally while the resonant frequency increases (from 6.48 GHz to 9.08 GHz) with applied dc magnetic field. Since the nonbiased ferrite behaves as a lossy dielectric, losses are reduces by as much as 0.4 dB in the biased state.

Finally, Fig. 6*a* and *b* shows E-plane and H-plane results, respectively, for a rectangular patch on a substrate material with biaxial ε and μ characteristic as given in (1) and (2). The substrate height is chosen as parameter. The dependence in the E plane (Fig. 6(a)) is such that with increasing substrate height, losses increase and the resonant frequency decreases. Following the reasoning applied to the results in Fig. 4, the E-plane beamwidth should be enlarged due to reduction in resonant frequency, i.e., the reduction of the effective aperture. However, the opposite tendency is observed here, which we attribute to the tensor coupling between x and z field components. Interestingly enough, the characteristic is reversed in the H-plane pattern (see Fig. 6(b))—except for the resonant frequency, of course. This effect might be used in future applications involving new material developments to arrive at almost identical E- and H-plane patterns for a single patch radiator.

IV. CONCLUSION

An extended spectral-domain immittance approach for the calculation of resonant frequencies and radiation patterns of rectangular patch antennas is presented. The modifications introduced are geared toward the incorporation of material parameters to be encountered in modern and future integrated-circuit fabrication procedures. These include the influences of electrically and magnetically biaxial substrates, the losses of the radiating patch as well as those of the ground metallization, and, at the same time, the possibility to analyze

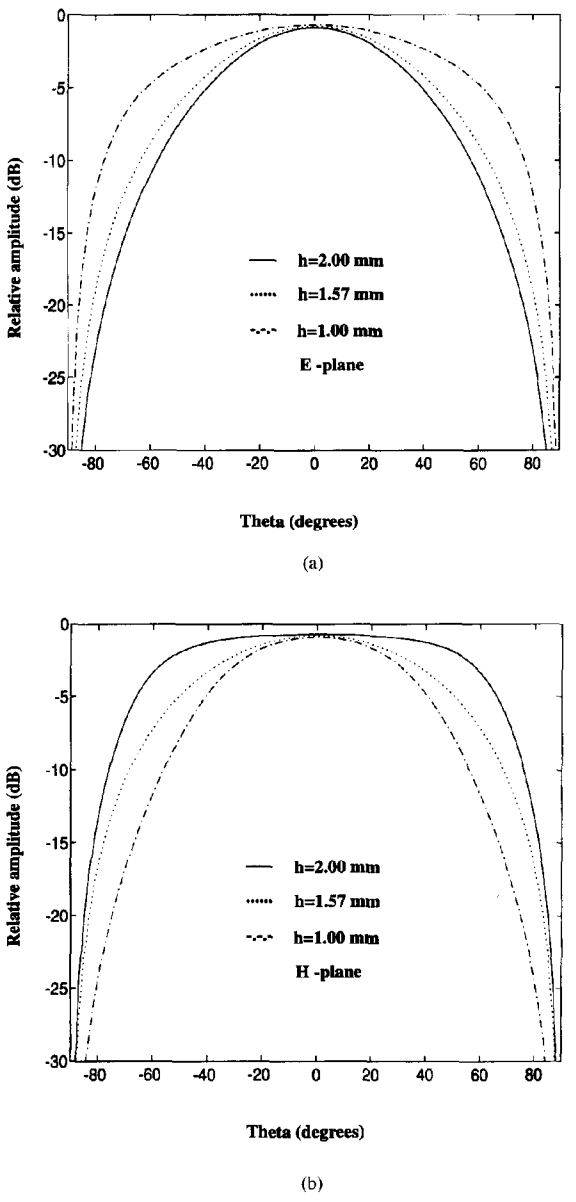

Fig. 6. Influence of substrate height of biaxial material on radiation pattern. Parameters: $W = 5$ mm, $L = 10$ mm, $\tan\delta = 0.001$, $\varepsilon_x = 4.35$, $\varepsilon_y = 2.35$, $\varepsilon_z = 0.2$, $\mu_x = 1.8$, $\mu_y = 1.4$, $\mu_z = 0.3$, $t_1 = t_2 = 5$ μm, $\sigma_1 = \sigma_2 = 40$ S/μm; dash-dotted lines: $h = 1$ mm, $f_0 = 14.8$ GHz; dotted lines: $h = 1.57$ mm, $f_0 = 13.9$ GHz; solid lines: $h = 2$ mm, $f_0 = 12.4$ GHz. (a) E plane, (b) H plane.

high-Tc superconductors as a frequently proposed alternative to conventional patch radiators. Another advantage of this method is that even for substrates with both permeability and permittivity tensors, the transformed electromagnetic field can be decoupled with respect to TE-to-y and TM-to-y waves, which directly leads to closed-form expressions for the transverse propagation constants and related immittances. Therefore, the method is CPU-time efficient, and the software is operational on modern workstations. The results presented demonstrate first that anisotropies and losses have an effect on beamwidths and resonant frequencies, and second that these parameters must be taken into account for modern and future integrated-circuit antenna designs.

REFERENCES

[1] N. G. Alexopoulos, "Integrated-circuit structures on anisotropic substrate," *IEEE Trans. Microwave Theory Tech.*, vol. MTT-33, pp. 847–881, Oct. 1985.

[2] R. C. Hansen, "Antenna application of superconductors," *IEEE Trans. Microwave Theory Tech.*, vol. 39, pp. 1508–1512, Sept. 1991.

[3] R. M. Nelson, D. A. Rogers, and A. G. D'Assunção, "Resonant frequency of a rectangular microstrip patch on several uniaxial substrates," *IEEE Trans. Antennas Propagat.*, vol. 38, pp. 973–981, July 1990.

[4] D. M. Pozar, "Radiation and scattering from a microstrip patch on a uniaxial substrate," *IEEE Trans. Antennas Propagat.*, vol. AP-35, pp. 613–621, June 1987.

[5] C. M. Krowne, "Relationships for Green's function spectral dyadics involving anisotropic imperfect conductors imbedded in layered anisotropic media," *IEEE Trans. Antennas Propagat.*, vol. 37, pp. 1207–1211, Sept. 1989.

[6] H. Chaloupka *et al.*, "Miniaturized high-temperature superconductor microstrip patch antenna," *IEEE Trans. Microwave Theory Tech.*, vol. 39, pp. 1513–1521, Sept. 1991.

[7] Z. Cai and J. Bornemann, "Generalized spectral-domain analysis for multilayered complex media and high-Tc superconductor applications," *IEEE Trans. Microwave Theory Tech.*, vol. 40, pp. 2251–2257, Dec. 1992.

[8] Z. Cai and J. Bornemann, "Full-wave analysis of high-Tc superconductor patch antenna on lossy bi-anisotropic substrates," in *1992 IEEE-APS Int. Symp. Dig.*, pp. 983–986.

[9] T. Itoh, "Spectral-domain immittance approach for dispersion characteristics of generalized printed transmission lines," *IEEE Trans. Microwave Theory Tech.*, vol. MTT-28, pp. 733–736, July 1980.

[10] T. Itoh and W. Menzel, "A full wave analysis method for open microstrip structures," *IEEE Trans. Antennas Propagat.*, vol. AP-29, pp. 63–67, Jan. 1981.

[11] D. Nghiem, J. T. Williams, and D. R. Jackson, "A general analysis of propagation along multiple-layer superconducting stripline and microstrip transmission lines," *IEEE Trans. Microwave Theory Tech.*, vol. 39, pp. 1553–1565, Sept. 1991.

[12] D. M. Sheen, S. M. Ali, D. E. Oates, R. S. Withers, and J. A. Kong, "Current distribution resistance, and inductance for superconducting strip transmission lines," *IEEE Trans. Appl. Superconductivity*, vol. 1, pp. 108–115, June 1991.

[13] E. Chang, S. A. Long, and W. F. Richards, "An experimental investigation of electrically thick rectangular microstrip antennas," *IEEE Trans. Antennas Propagat.*, vol. AP-34, pp. 767–772, June 1986.

[14] D. Polder, "On the theory of ferromagnetic resonance," *Phil. Mag.*, vol. 40, pp. 99–115, 1949.

[15] J. J. Green and F. Sandy, "Microwave characterization of partially magnetized ferrites," *IEEE Trans. Microwave Theory Tech.*, vol. MTT-22, pp. 642–645, June 1974.

[16] Z. Cai and J. Bornemann "Spectral-domain analysis of patch radiators on lossy ferrite substrates," in *Proc. 1993 ACES Conf.*, pp. 821–827, Mar. 1993.